Thesis Summary

論文題目　**Application of unimodal-distributed morphological parameters for phenotyping of the budding yeast**

(単峰性分布をする形態パラメータを使った出芽酵母のフェノタイピング)

氏　　名　　ガーネゴルモハンマディ　ファルザン

Introduction

Morphology is a basic phenotypic characteristic of organisms/cells that can be affected by genetic and/or environmental perturbations. Rapid advancements in image-processing software enable acquiring quantitative morphological data of eukaryotic cells. For example, CalMorph has been widely-used for high-dimensional morphological phenotyping of budding yeast, *Saccharomyces cerevisiae*. Cells respond to a perturbation among a wide range of values; hence, cell populations are usually multimodal (i.e., mixed population). Multimodality increases the complexity of the statistical model, and therefore, valid statistical approaches are in high demand for morphological phenotyping. However, it still remained uncertain that morphological parameters extracted by CalMorph are unimodal. In this study, I attempted to detect unimodal parameters among the 501 CalMorph morphological parameters. By using all unimodal morphological parameters, generalized linear model (GLM) was applied to find a novel functional domain in the catalytic subunit of 1,3-β-Glucan Synthase (GS) and to cluster 32 cell wall mutants defective in mannoproteins. This study provides a new valid approach for single-cell and population-levels morphological phenotyping.

Results and discussion

1. Multimodality in CalMorph parameters

In order to check modality of morphological traits quantified by CalMorph, I employed a standard morphological data set of wild-type budding yeast cells (BY4743, n = 114), after staining of the cell wall, actin, and nuclear DNA. Probabilistic mixture modeling methods were used to check whether every 501 trait is truly unimodal. As a result, 426 were found unimodal (Figure 1A). Integration of confounding factors (a group of five

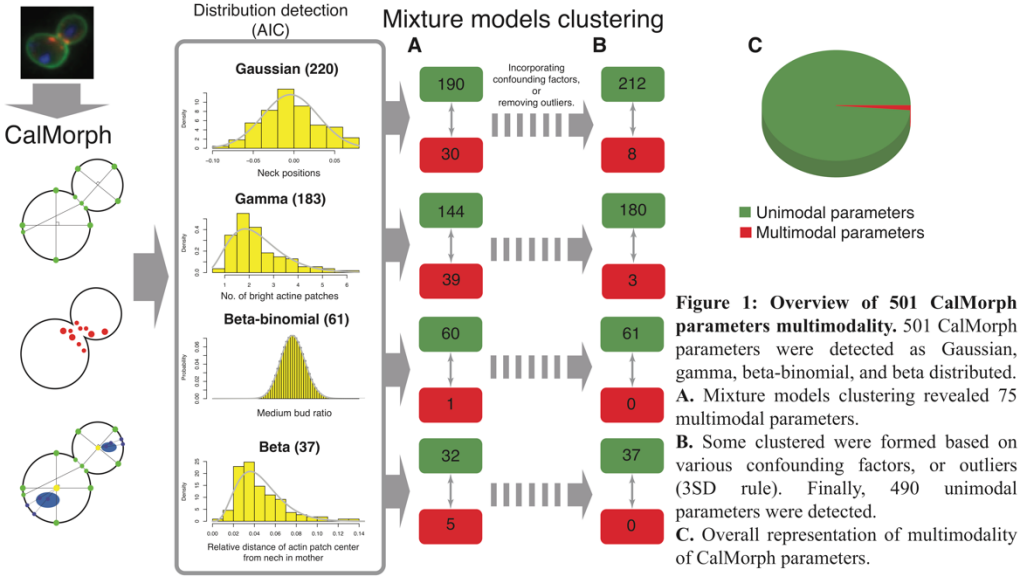

Figure 1: Overview of 501 CalMorph parameters multimodality. 501 CalMorph parameters were detected as Gaussian, gamma, beta-binomial, and beta distributed. **A.** Mixture models clustering revealed 75 multimodal parameters. **B.** Some clustered were formed based on various confounding factors, or outliers (3SD rule). Finally, 490 unimodal parameters were detected. **C.** Overall representation of multimodality of CalMorph parameters.

factors including employed microscopes and period of image acquisition) into the statistical model or removing outliers (3SD rule; Caicedo et al., 2017, *Nat Methods*) explained multimodality in 64 out of 75 parameters (i.e., AIC of confounding factor model was lower than the null model or outliers had formed individual distributions). Accordingly, 490 unimodal parameters were detected (Figure 1B) and further utilized for the morphological phenotyping. Overall, 98.7% CalMorph parameters are unimodal (Figure 1C). This study proposes a new approach for valid statistical analysis to assess morphological data generated by CalMorph.

2. Classification of *fks1*-temperaturesensitive mutants with GLM and Gaussian mixture model (GMM)

I used 490 unimodal parameters for clustering analysis of the temperature-sensitive GS mutants. For this purpose, I applied GLM and GMM to previously-obtained 5 replicates data of 10 *fks1-ts fks2*Δ GS mutant cells cultivated at 25ºC and 37ºC. After linear transformation with GLM, the significant morphological abnormality was assessed by Wald-test. Of 490 unimodal parameters, 353 parameters showed a statistically significant difference at least in one mutant compared with the null distribution (FDR < 0.05). The first three principal components (PC; covering 73.41% of the variation of the data set) were subjected to GMM clustering to identify four morphological clusters (Figure 2A). The validity of the obtained clusters was checked by randomization (2000 iterations), followed by Jaccard coefficient test (P= 5e-04). I found that the clustering analysis provided a new single cluster for *fks1-1093* (Y710H) which was not previously identified (Okada et al., 2010; *Genetics*). By application of Linear Discriminant Analysis (LDA), I also found that *fks1-1093* exhibited a specific morphological feature, having a significantly higher proportion of cells with two nuclei (Wald-test, P = 4.17e-17; Figure 2B). Therefore, the most probable explanation for the *fks1-1093* phenotype would be defects in bud morphogenesis. Overall, recent advancements in tools for analyzing morphological data enabled me to discover a new function of GS in bud morphogenesis (Figure 2C).

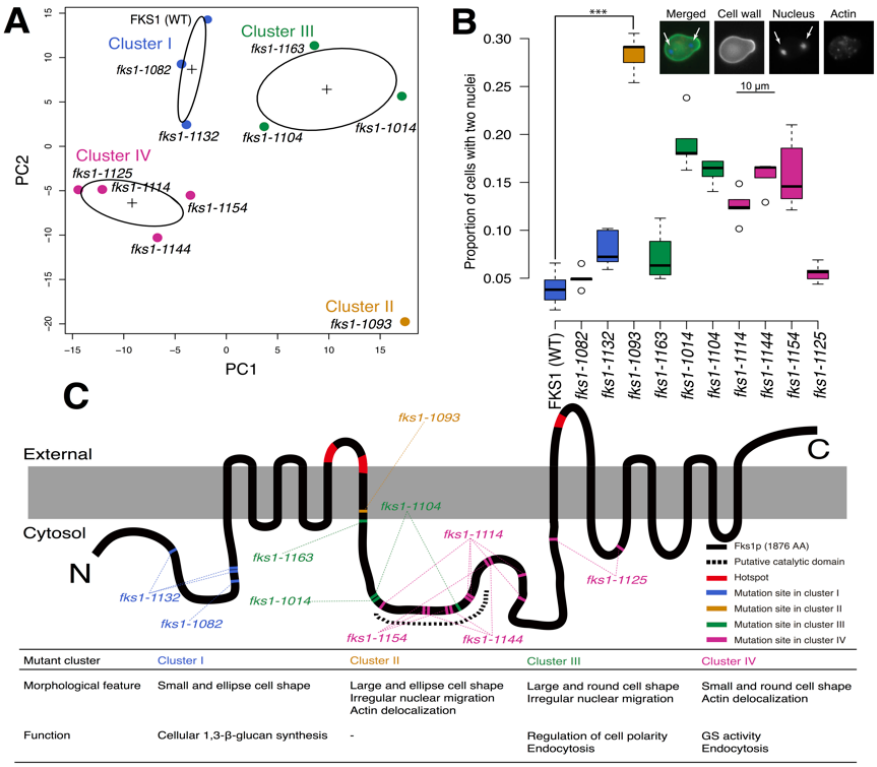

Mutant cluster	Cluster I	Cluster II	Cluster III	Cluster IV
Morphological feature	Small and ellipse cell shape	Large and ellipse cell shape Irregular nuclear migration Actin delocalization	Large and round cell shape Irregular nuclear migration	Small and round cell shape Actin delocalization
Function	Cellular 1,3-β-glucan synthesis	-	Regulation of cell polarity Endocytosis	GS activity Endocytosis

Figure 2: Morphological clustering of *fks1-ts* mutants. A. GMM clustering. **B.** Proportion of two nuclei. Inset: Arrows indicate nucleus. **C.** Functional dissection of Fks1p (modified from Okada et al., 2014; *MBoC*). The gray box denotes the plasma membrane. Mutation points are color-coded according to GMM clustering.

3. Morphological phenotyping of cell wall mutants

Broad outlines of yeast cell wall construction and regulation have been deciphered, but due to the complexity of the system, many open questions are remained obscure for a global understanding of the yeast cell wall. Attempts were made to uncover responsibility matrix of each mannoprotein by morphological phenotyping through my proposed approach; thus, a morphological data set of mutants defective in 26 glycosylphosphatidylinositol (GPI)- and 6 non-GPI-cell wall mannoproteins (Orlean, 2012, *Genetics*) were collected (Liu, unpublished). Morphological abnormalities in the cell wall mutants (n=5) were checked by comparing with the wild-type strain (n=21) for each parameter after applying an ANOVA model. Of 490 unimodal parameters, 134 parameters showed a significant difference at least in one mutant (Wald-test, FDR < 0.05). GMM clustering of the first five PC scores (covering 79.97% variation of the population) found a mixture of nine Gaussian distributions (Figure 3A). The validity of the obtained clusters was checked by randomization with 2000 iterations, followed by Jaccard coefficient test (*P*=5e-04). Among the nine clusters, members of five clusters (I, V, VI, VII, and IX; seven mutants in total) displayed obvious morphological defects, well explained by the functional defects of these proteins. Cluster I (*ccw12*Δ) mutation resulted in pleiotropic morphological defects, including wide neck (typical phenotype of cell wall mutants), round cell shape, and small buds. This is probably because Ccw12p is a main structural constituent of the cell wall (in average 190,716 molecules per cell). Cluster V (*egt2*Δ, *dse2*Δ and *sun4*Δ) mutations caused the accumulation of large budded cells before cell separation. These genes all encode glycosidases required for septum digestion, and therefore, it is likely that daughter cells do not separate due to remaining connection. Gene function of *ECM33* (cluster VI) has been unknown. But it may have a function in apical bud growth because the *ecm33*Δ mutant exhibited an accumulation of round small buds (Figure 3B). The possible function of cluster VII (*FIG2*) and cluster IX (*SAG1*) genes in mating were previously suggested, but their roles in the vegetative growth phase are still unknown. Morphological phenotyping revealed that both mutants were defective in actin organization. Genetic interactions of *FIG2* (cluster VII) and *SAG1* (cluster IX) (Costanzo et al., 2016, *Science*) showed that *FIG2* negatively interacts with *ACT1* (actin gene) and *BNI1* (formin

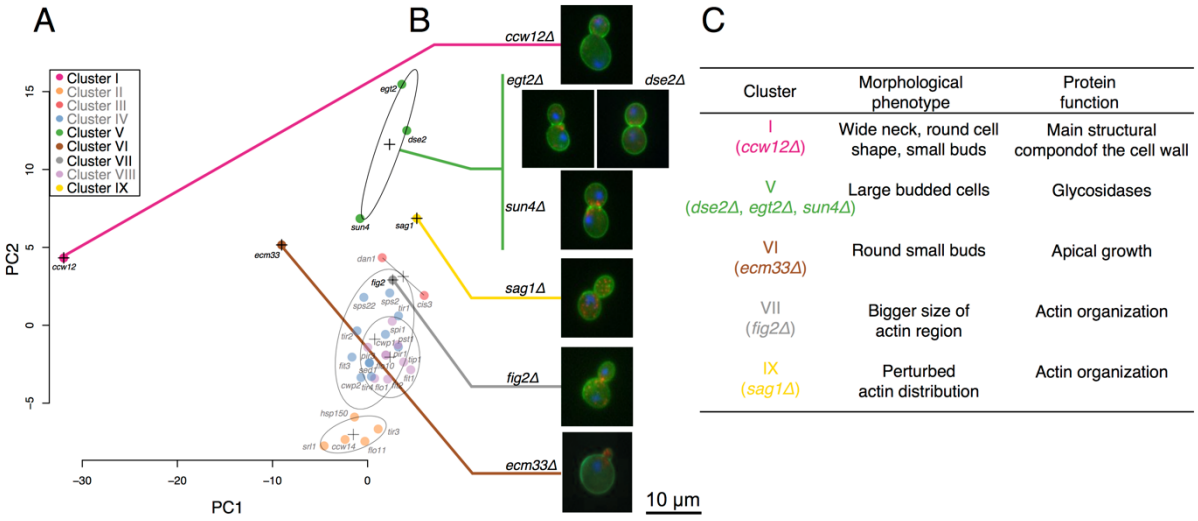

Figure 3: Morphological phenotyping of cell wall mutants. A. GMM clustering results. **B.** Images of five clusters with distinct morphological changes. Cells were stained with FITC for cell wall (green), rhodamine for actin (red), and DAPI for nuclear DNA (blue), and presented with pseudo-coloring. **C.** Morphological defects and molecular function of genes causing apparent morphological defects.

component required for actin assembly); *SAG1* negatively interacts with *COF1* (encoding actin-binding protein, cofilin) and *PFY1* (encoding actin-binding protein, profilin). So, it is likely that clusters VII and IX (*FIG2* and *SAG1*, respectively) genes are somehow and differently responsible for the actin function (Figure 3C).

Conclusions

1. Among 501 morphological parameters of CalMorph, I identified 490 unimodal-distributed parameters. In combination with GLM and parametric analysis, they provide a sensitive approach to assess morphological phenotyping, setting up a new valid foundation for the phenome studies.
2. Application of unimodal-distributed morphological parameters and GMM clustering revealed a new functional domain in Fks1p involved in bud morphogenesis.
3. My proposed approach was also useful to decipher distinct roles of yeast cell wall mannoproteins. Morphological features caused by the defects of some mannoproteins (including Ccw12p, Egt2p, Dse2p, Sun4p, Ecm33p, Fig2p and Sag1p) can be explained by their molecular functions.

References

1. **Ghanegolmohammadi F**, Ohnuki S, and Ohya Y (2019) Single-Cell Phenomics in Budding Yeast: Technologies and Applications. Single-Cell Omics Vol. 1, *Elsevier* (book chapter, in press).
2. **Ghanegolmohammadi F**, Shobbar ZS, Pourabed E and Ghanatir F (2017) UTR analysis of bZIP transcription factor family in barley. *Agricultural Biotechnology*, 7(2): 45-52.